UAV-based system for real-time wildfire perimeter propagation tracking

Constantinos Heracleous, Panayiotis Kolios and Christos G. Panayiotou

Abstract— **Real-time wildfire perimeter tracking provides situational awareness and enhances decision-making during firefighting. This paper proposes a UAV-based system that integrates real-time data collection (using onboard sensors) into a fire propagation model to provide accurate state information on the wildfire perimeter and improve fire prediction. Firstly, a data fusion scheme is devised to employ available historical data in combination with real-time measurements to provide updated inputs to the fire propagation model. Then the model is used to predict the future fire perimeter and uses these predictions to guide the UAV to track the fire perimeter better. The proposed system is evaluated in extensive simulation experiments, demonstrating its effectiveness for real-time wildfire perimeter propagation tracking.**

I. INTRODUCTION

In recent years, climate change has created conditions with warmer temperatures, prolonged droughts, and changes in precipitation patterns that made wildfires more frequent, intense, and challenging to predict and control [1]. According to the latest EFFIS annual report [2], 2022 was the year with the highest number of fires since 2006 and the most severe drought recorded in Europe over the last 500 years. The area burnt surpassed 8600 km^2, which is the largest area burnt by wildfires in the EU since 2006.

Firefighting requires early detection, accurate propagation estimation, and continuous tracking [3]. Furthermore, real-time information for the wildfire state provides situational awareness and enhances decision-making in designing suitable action plans to curb fire spreading and call for evacuation procedures when deemed unavoidable [4].

In addition, the increasing availability and extensive capabilities of unmanned aerial vehicles (UAVs) have made them ideal for real-time wildfire monitoring. Compared to common wildfire monitoring methods, such as satellite image inspection and using helicopters or other manned aerial vehicles, UAVs possess significant advantages. They conserve sizeable operational costs and minimize risks compared to manned aerial vehicles. Also, they are available on-demand with various sensors onboard to provide real-time coverage compared to the satellites' periodic coverage and generally long revisit times.

UAVs received significant attention from the research community for tackling the wildfire propagation tracking problem, with several UAV-based methods proposed and reviewed over the recent years [5]–[8]. The use of UAVs for wildfire tracking was initially studied in [3], where the authors proposed a cooperative control method for monitoring the fire perimeter using a team of UAVs. The main objective was to minimize the information latency and the frequency of updates to the mission base station by guiding the UAVs in clockwise and counterclockwise directions around the fire perimeter. The fire perimeter tracking problem was also studied in [9], with the authors proposing cooperative control for a team of UAVs based on optimizing utility functions keeping the UAVs close to the fire boundary.

In [10], the authors develop an importance-based coordination method for wildfire monitoring using multiple UAVs. Specifically, rather than monitoring the whole fire perimeter with the same frequency as in the previously discussed methods, the UAVs are controlled to visit the higher-importance perimeter points more frequently based on their fire spread rate. Similarly, the work in [11] focuses on controlling a network of UAVs to monitor only the faster-moving segment of the fire frontier. To achieve this task, the authors design a sliding-mode control algorithm that moves the UAVs to the faster-moving region of the fire according to an optimization setup.

The authors in [4] proposed a distributed control framework that enables a team of UAVs to monitor collaboratively the wildfire propagation. Specifically, by minimizing the information loss from the UAVs cameras associated with quantified fire heat intensity levels, the UAVs can monitor the perimeter as it spreads while maintaining coverage of the whole wildfire. The work in [12] proposes a distributed control framework for navigating a team of UAVs to monitor the wildfire spreading while at the same time considering the areas of firefighter activity. The authors first generate a fire-front uncertainty map and a human uncertainty map from the GPS signal received by the firefighters. Then by minimizing a dual-criteria objective function, they derive the positions that the UAV agents must navigate to monitor the fire and sense the firefighters. Finally, the authors in [13] proposed a UAV-based system that monitors the wildfire evolution but is also able to periodically fly ahead of the fire and collect valuable data that can be used to anticipate better the fire behavior and movement.

In comparison to the previous works, in this paper, we investigate a UAV-based system that combines the UAV's

*This work was undertaken as part of the GLIMPSE project EXCELLENCE/0421/0586 which is co-financed by the European Regional Development Fund and the Republic of Cyprus through the Research and Innovation Foundation's RESTART 2016-2020 Programme for Research, Technological Development and Innovation and supported by the European Union's Horizon 2020 research and innovation programme under grant agreement No 739551 (KIOS CoE), and from the Government of the Republic of Cyprus through the Cyprus Deputy Ministry of Research, Innovation and Digital Policy.

The authors are with KIOS Research and Innovation Center of Excellence and the Department of Electrical and Computer Engineering, University of Cyprus, Nicosia, Cyprus. con.heracleous@gmail.com, pkolios@ucy.ac.cy, christosp@ucy.ac.cy

sensing capabilities and a wildfire propagation model to provide real-time state information on the wildfire perimeter. This method enables the UAV to move over areas where the uncertainty of the fire propagation is minimized and thus more accurately and efficiently track the fire perimeter. Specifically, the proposed system consists of a UAV capable of measuring the fire perimeter, fuel type, and weather conditions. A data fusion scheme is devised that fuses available historical data with real-time measurements, providing more accurate inputs to a wildfire model. The wildfire model provides real-time estimates of the future perimeter state used by the wildfire perimeter tracking scheme that guides the UAV towards trajectories that minimize the error between the anticipated and actual wildfire perimeter. A guidance and control scheme is employed to enable the UAV to follow the calculated trajectories efficiently and receive the desired measurements.

The rest of this paper is organized as follows. Section II describes the wildfire propagation model employed in this work, and Section III formulates the problem. Section IV derives the proposed UAV-based system for real-time wildfire perimeter propagation tracking. Finally, Section **??** presents simulation results illustrating the effectiveness of the proposed method, and Section VI provides some concluding remarks.

II. WILDFIRE MODELING

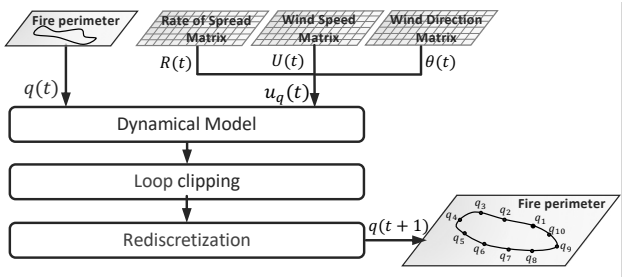

Fig. 1. Wildfire model.

In this work, we utilize the works in [14]–[16] to implement a simplified version of the FARSITE model [17] that requires fewer input data and can still represent a realistic surface fire propagation. Specifically, the simplified wildfire model takes as inputs the steady-state of fire spread rate, the wind speed, and wind direction, all represented in a discrete grid base environment, and calculates the propagation of fire fronts that are denoted as vertices connected in a counterclockwise direction forming the fire perimeter. Fig. 1 illustrates the main parts of the simplified fire model, which we describe in the sequel.

A. Dynamical model

The propagation of each fire-front in the 2D plane is calculated using the following discrete-time dynamical model:

$$q_i(t+1) = q_i(t) + \Delta t Q_i(t), \quad \forall i = 1, \cdots, N(t), \qquad (1)$$

where $q_i = [x_i, y_i]^T$ are the cartesian coordinates of i-th fire-front vertex with initial location $q_i(0) = q_0^i$ while Δt is the time step. $N(t)$ denotes the number of fire-fronts in the perimeter at time t with $q_1(t) = q_{N(t)}(t)$. $Q_i = [X_i, Y_i]^T$ are the orthogonal spread rate differentials (m min^{-1}) given in (2) at the bottom of the page, where θ is the angle (rad) of the wind direction and vertical axis ($0 \leq \theta < 2\pi$) increasing clockwise, $x_s = x_{i+1} - x_{i-1}$ and $y_s = y_{i+1} - y_{i-1}$ denote the component differentials representing the orientation of the i-th vertex on the fire-front, while a, b and c (m min^{-1}) describe the shape of an elliptical fire at each vertex calculated as follows:

$$a = \frac{0.5(R + \frac{R}{HB})}{LB}, \; b = \frac{(R + \frac{R}{HB})}{2}, \; c = b - \frac{R}{HB} \qquad (3)$$

where R is the fire spread rate (m min^{-1}), HB is the head to back ratio given as $HB = \frac{LB+(LB^2-1)^{0.5}}{LB-(LB^2-1)^{0.5}}$, and LB is the length to breadth ratio given as $LB = 0.936e^{0.2566U} + 0.461e^{-0.1548U} - 0.397$, with U denoting the the mid-flame wind speed (m s^{-1}).

B. Loop-clipping

As each fire-front propagates using (1), due to non-uniform inputs (i.e., rate of spread and weather), internal loops can be generated that affect the correct representation of the fire perimeter [17]. These loops need to be clipped before rendering the fire perimeter unusable. Therefore, at each time step, a loop-clipping algorithm has been implemented that checks if any segments of the perimeter intersect, causing an internal loop, and removes them appropriately to keep the perimeter usable.

C. Rediscretization

As the wildfire propagates, the distance between subsequent fire-front vertices increases, creating an error in the calculation of the perimeter, especially in the case of non-uniform spread rates where sharp curves in the perimeter are possible. To eliminate these errors, new vertices need to be added to the perimeter sections with high curvature. The following condition is used for determining where to add new vertices [14]:

$$\max\left(\cos\frac{\beta_i}{2}, \cos\frac{\beta_{i-1}}{2}\right) > \left(\frac{T_l}{l_i}\right)^2 \qquad (4)$$

$$X_i = \frac{a^2\cos\theta(x_s\sin\theta + y_s\cos\theta) - b^2\sin\theta(x_s\cos\theta - y_s\sin\theta)}{\sqrt{b^2(x_s\cos\theta - y_s\sin\theta)^2 + a^2(x_s\sin\theta + y_s\cos\theta)^2}} + c\sin\theta,$$
$$Y_i = \frac{-a^2\sin\theta(x_s\sin\theta + y_s\cos\theta) - b^2\cos\theta(x_s\cos\theta - y_s\sin\theta)}{\sqrt{b^2(x_s\cos\theta - y_s\sin\theta)^2 + a^2(x_s\sin\theta + y_s\cos\theta)^2}} + c\cos\theta. \qquad (2)$$

where β_i is the angle between the segments of vertices q_{i+1}, q_i, q_{i-1}, and similarly β_{i-1} can be calculated. $l_j = \|q_i - q_{i-1}\|$ is the distance between the subsequent vertices q_i and q_{i-1}, and T_l is a positive specified threshold parameter. If the above condition is true in any line segment of the perimeter, then a new vertex is added at the midpoint of that segment (i.e., $\frac{l_i}{2}$), while the condition is used recursively to the new segment halves and new vertices are added until the condition in (4) is satisfied by all the new points between the vertices q_i and q_{i-1}.

D. Complete Wildfire model

The complete wildfire model, as illustrated in Fig. 1, can be represented by the following discrete-time function:

$$q(t+1) = f\big(q(t), u_q(t)\big), \tag{5}$$

where $q = [q_1, \ldots, q_{N(t)}]^T$ are the perimeter vertices as described in (1), and $u_q = [R, U, \theta]$ are the input matrices $R, U, \theta \in \mathbb{R}^{n_x \times n_y}$ with R denoting the steady-state of fire spread rate, U the mid-flame wind speed, and θ the wind direction. Finally, function f includes the dynamical model in (1) and the loop-clipping and rediscretization algorithms as described above.

III. PROBLEM FORMULATION

Using the wildfire propagation model described in Section II, we aim to develop a UAV-based system that allows accurate real-time tracking of the wildfire perimeter.

As the wildfire propagates and enlarges, the UAV and its onboard camera, through its field of view (FOV), take measurements from sections of the perimeter over consecutive time instances. Of course, relying only on collected measurements can lead to inaccurate and delayed fire perimeter state information over time, especially in the fast-moving segments of the fire. To address this issue the wildfire model as described in Section II is used to predict the wildfire perimeter and updated based on the UAV real-time measurements. Thus, it is necessary to devise a scheme that guides the UAV to specific perimeter locations for measurements that will not only depict the growing fire fronts but also update the model in order to further more accurately predict the future fire fronts and more appropriately guide the UAV to its next locations.

To help with the problem formulation, Fig. 2 shows a segment snapshot of the wildfire perimeter, the simulated perimeter, and the measured perimeter. Considering the wildfire perimeter $q = [q_1, \ldots, q_N]$ and the simulated perimeter $\hat{q} = [\hat{q}_1, \ldots, \hat{q}_{\hat{N}}]$ the mean error distance between the two at time t can be calculated as

$$\varepsilon_d(t) = \frac{1}{N_d(t)} \sum_{i=1}^{N_d(t)} d_i(t) \tag{6}$$

where d_i, $i = 1, \ldots, N_d$, as shown in Fig. 2, is the i-th distance between wildfire and simulated perimeter segments calculated using

$$d_i(t) = \|\hat{\varrho}_i(t) - \varrho_i(t)\| \tag{7}$$

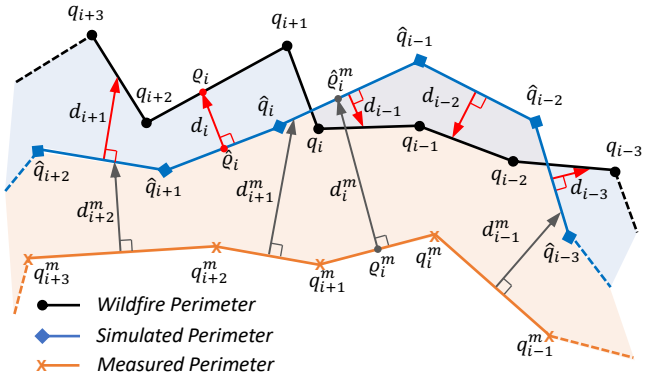

Fig. 2. Wildfire perimeter segment snapshot in 2D with the simulated perimeter and the measured perimeter illustrating the distance between them.

with $\hat{\varrho}_i = \frac{\hat{q}_{i+1}+\hat{q}_i}{2}$ and ϱ_i is the intersection of the perpendicular line extended from $\hat{\varrho}_i$ to the wildfire perimeter.

Similarly, considering the simulated perimeter $\hat{q} = [\hat{q}_1, \ldots, \hat{q}_{\hat{N}}]$ and the measured perimeter $q^m = [q_1^m, \ldots, q_{N_m}^m]$ the mean error distance between the two at time t can be calculated as

$$\varepsilon_{d^m}(t) = \frac{1}{N_{d^m}(t)} \sum_{i=1}^{N_{d^m}(t)} d_i^m(t) \tag{8}$$

where d_i^m, $i = 1, \ldots, N_{d^m}$, as shown in Fig. 2, is the i-th distance between simulated perimeter segments and measured perimeter calculated using

$$d_i^m(t) = \|\varrho_i^m(t) - \hat{\varrho}_i^m(t)\| \tag{9}$$

with $\varrho_i^m = \frac{q_{i+1}^m + q_i^m}{2}$ and $\hat{\varrho}_i^m$ is the intersection of the perpendicular line extended from ϱ_i^m to the simulated perimeter.

The main objective is to minimize the mean error distance of the simulated perimeter from the measured perimeter by guiding the UAV to take measurements from specific locations of the wildfire perimeter. Specifically, we would like to minimize the following:

$$\min_{d^m(t)} \varepsilon_{d^m}(t), \tag{10}$$

which subsequently will minimize the mean error $\varepsilon_d(t)$ between the wildfire perimeter and the simulated perimeter.

To achieve this objective, we propose a UAV-based system that is able to track the wildfire by simulating its perimeter and determining specific locations for the UAV to take measurements so that the simulated perimeter is updated and provides an accurate state of the actual wildfire.

IV. PROPOSED SYSTEM

The proposed UAV-based wildfire perimeter tracking system is depicted in Fig. 3 and consists of five modules, the Unmanned Aerial Vehicle (UAV), the Wildfire Model (WM), the Wildfire Perimeter Tracking (WPT), the Guidance and Control (GC) and the Data Fusion (DF) that we describe in the sequel.

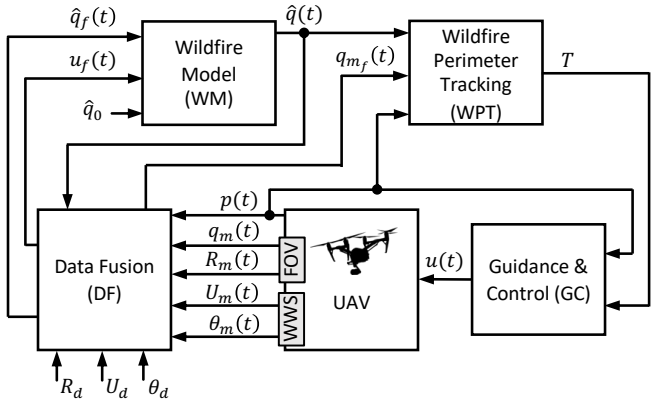

Fig. 3. The proposed UAV-based real-time wildfire perimeter tracking system architecture.

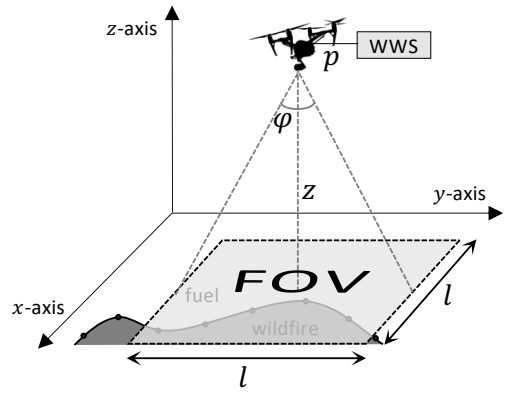

Fig. 4. The UAV through its field of view (FOV) can measure the wildfire perimeter and identify the fuel type, and through its wind and weather sensor (WWS) can measure wind speed and direction.

A. Unmanned Aerial Vehicle

The UAV is free to fly in the 3D space and at a safe altitude from the fire. Let $p = [x, y, z]^T \in \mathbb{R}^3$ denote the position of the UAV in the 3D space, where $[x, y] \in \mathbb{R}^2$ denotes the 2D plane coordinates while $z \in \mathbb{R}$ denotes the altitude. The following discrete-time linear dynamical model is used for the evolution of the UAV agent in the 3D space:

$$p(t+1) = p(t) + u(t)\Delta t, \tag{11}$$

where Δt is the time step and $u \in \mathbb{R}^3$ is the control input that is represented by the speed vector $u = [u_x, u_y, u_z]^T$.

The UAV is equipped with a camera that is attached at the bottom of the UAV, enabling fire perimeter measurement, and also we assume that has the capability of fuel type (e.g., vegetation) identification that allows spread rate prediction [18]. The camera has a square field of view (FOV) as shown in Fig. 4, with side length l that is given by:

$$l(t) = 2z(t)\tan\frac{\varphi}{2}, \tag{12}$$

where $z \in p$ is the UAV altitude, and $\varphi = 2\tan^{-1}\frac{S}{2F}$ is the angular FOV with S denoting the sensor size, and F is the lens focal length both available from the camera specifications. Also, the UAV is equipped with a wind and weather sensor (WWS) that is capable of measuring the wind speed and direction as it flies in 3D space. Therefore, using its onboard sensors, the UAV acquires through its FOV real-time measurements for the fire-front position $q_m(t)$ and the fire spread rate $R_m(t)$, and also through WWS measurements for the wind speed $U_m(t)$ and wind direction $\theta_m(t)$.

B. Wildfire Model

The system utilizes the wildfire model as described in Section II to simulate the wildfire perimeter in real-time using fused historical data and UAV real-time measurements after processing by the DF module. Specifically, for simulating the wildfire, similar to (5), the following discrete-time dynamical model is used

$$\hat{q}(t+1) = f\big(\hat{q}_f(t), \hat{u}_f(t)\big), \tag{13}$$

where $\hat{q} = [\hat{q}_1, \ldots, \hat{q}_{\hat{N}(t)}]^T$ are the simulated perimeter vertices, while $\hat{q}_f$ are the fused perimeter vertices and $u_f = [R_f, U_f, \theta_f]$ are the fused input matrices both coming from the DF module that is described in the sequel. The simulated wildfire perimeter is the proposed system output. It is provided to the firefighting mission commander since it is the closest estimate of the actual wildfire perimeter, as illustrated in the simulation results in Section **??**.

C. Wildfire Perimeter Tracking

The WPT module is responsible for calculating a trajectory $T = [w_1, \ldots, w_j, \ldots, w_{N_T}]$, where $w_j = [x_j, y_j, z_j]$ is the j-th waypoint, that the UAV can follow and take measurements for minimizing (10). Initially, a trajectory is calculated once the UAV reaches the wildfire and then a new trajectory is calculated every time the UAV reaches the final waypoint of the current trajectory i.e., w_{N_T}.

Algorithm 1 Wildfire Perimeter Tracking (WPT) module

1: **Input:** $\hat{q}(t)$, $q_{m_f}(t)$, $p(t)$
2: **Output:** $T = [w_1, \ldots, w_{N_T}]$
3: **if** UAV reached final waypoint **then**
4: $[w^p, d^m, w_T, d_T] \leftarrow$findPosWaypoints$\big(\hat{q}(t),\, q_{m_f}(t)\big)$
5: $A \leftarrow$ generateAdjacencyMatrix$(w_p, p(t))$
6: $w_S \leftarrow p(t)$
7: $T \leftarrow$ dijkstra(A, w_S, w_T)
8: **end if**

WPT uses Algorithm 1 for calculating the trajectory T. Fig. 5 illustrates visually the process. Initially, the distance d^m between simulated $\hat{q}(t)$ and fused measured $q_{m_f}(t)$ perimeters is calculated similarly as described in Section III. Then the target distance is set as $d_T = 2\max(d^m)$ and based on (12) the UAV altitude, so that FOV covers adequately both perimeters, is calculated using

$$z_T = \frac{2sd_T}{\tan\frac{\varphi}{2}}, \tag{14}$$

where $s \geq 1$ is a user-defined scaling factor parameter.

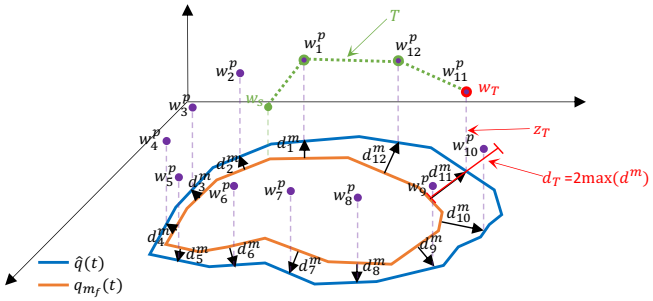

Fig. 5. Trajectory calculation by Wildfire Perimeter Tracking (WPT).

Subsequently, the possible waypoints w^p are calculated using the 2D coordinates of $\hat{\varrho}^m$ (i.e., the intersection points of the perpendicular line extended from ϱ^m points as described in Section III) at altitude z_T, i.e., $w_i^p = [\varrho_i^m, z_T]$. The target waypoint w_T is set as the waypoint above d_T.

Using the possible waypoints w^p and the UAV position $p(t)$ the adjacency matrix A is calculated next. The adjacency matrix is sparse since connections only between neighboring w^p are included with their distance as weight, i.e., $d_i^p = \left\| w_{i+1}^p - w_i^p \right\|$. Therefore, the UAV continuously follows the wildfire perimeter and is not crossing the wildfire. Finally, the trajectory T is calculated utilizing Dijkstra's shortest path algorithm with matrix A and as the start node the UAV current position $w_s = p(t)$, and as target node w_T.

D. Guidance and Control

The UAV trajectory tracking is handled by the Guidance and Control module that utilizes Algorithm 2. At each time step, the distance in each dimension (i.e., d_w^x, d_w^y, d_w^z as shown in Fig. 6) between the UAV position $p(t)$ and the current waypoint $w_i \in T$ that must be reached is calculated via $d_w(t) = w_i - p(t)$. Next, using the 3D polar coordinates system as shown in Fig. 6, the horizontal azimuth angle $\phi(t)$ measured on the xy plane from the x-axis is calculated (Alg. 2-line 10), and the azimuth angle $\theta(t)$ measured from the z axis (Alg. 2-line 11). Finally, the control speed vector is determined by calculating the speed in each dimension as shown in Alg. 2-lines 12-14 using the reference speed V_{ref} set by the user for the UAV. It's important to note that a waypoint (i.e., $w_i \in T$) is reached when $\|p(t) - w_i\| \leq \epsilon$, where $\epsilon = V_{\text{ref}}\Delta t$ is the distance error threshold, and the next waypoint $w_{i+1} \in T$ is set until the last waypoint $w_{N_T} \in T$ is reached and a new trajectory is calculated by WPT module.

Algorithm 2 Guidance and Control (GC) module

1: **Input:** $T = [w_1, \ldots, w_{N_T}]$, $p(t)$
2: **Output:** $u(t) = [u_x(t), u_y(t), u_z(t)]^T$
3: $i \leftarrow 1$
4: $\epsilon \leftarrow V_{\text{ref}}\Delta t$
5: **while** $\|p(t) - w_{N_T}\| > \epsilon$ **do**
6: **if** $\|p(t) - w_i\| \leq \epsilon$ **then**
7: $i \leftarrow i + 1$
8: **end if**
9: $d_w(t) \leftarrow w_i - p(t)$
10: $\phi(t) \leftarrow \tan^{-1}(\frac{d_w^y(t)}{d_w^x(t)})$
11: $\theta(t) \leftarrow \tan^{-1}(\frac{\sqrt{(d_w^x(t))^2 + (d_w^y(t))^2}}{d_w^z(t)})$
12: $u_x(t) = V_{\text{ref}} \cos\phi(t) \sin\theta(t)$
13: $u_y(t) = V_{\text{ref}} \sin\phi(t) \sin\theta(t)$
14: $u_z(t) = V_{\text{ref}} \cos\theta(t)$
15: **end while**

E. Data Fusion

The Data Fusion (DF) module is responsible for fusing the wildfire simulated perimeter with real-time wildfire perimeter measurements and also fusing available historical data for the fire spread rate, wind speed, and wind direction with real-time measurements from the UAV sensors.

Specifically, as the UAV tracks the wildfire following the calculated trajectory, the DF module fuses the simulated perimeter with the UAV perimeter measurements. Fig. 7 illustrates the DF module process for a perimeter segment. Fig. 7(a) shows the wildfire perimeter $q(t)$, the simulated perimeter $\hat{q}(t)$, and the fused measured perimeter $q_{m_f}(t)$ before the UAV arrives. Once, the perimeter segment is under the UAV FOV, the fire-front measurements $q_m(t)$ are fused with the already available perimeter measurements $q_{m_f}(t)$, as shown in Fig. 7(b). Subsequently, the fire-front measurements $q_m(t)$ are also fused with the simulated perimeter $\hat{q}(t)$ providing the fused simulated perimeter $\hat{q}_f(t)$, as shown in Fig. 7(c). The perimeter data fusion process requires updating correctly the vertices' order so that the accuracy of the perimeter is not affected causing calculation issues in the wildfire model. The perimeter data fusion process repeats for each perimeter segment in the UAV FOV providing continuously the fused simulated perimeter $\hat{q}_f(t)$ input data to the WM module.

The DF module also fuses data for fire spread rate, wind

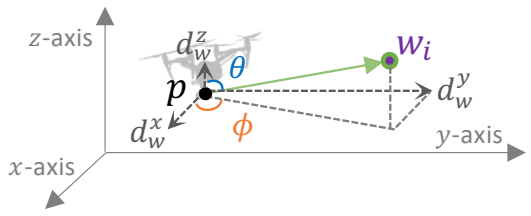

Fig. 6. 3D polar coordinates system.

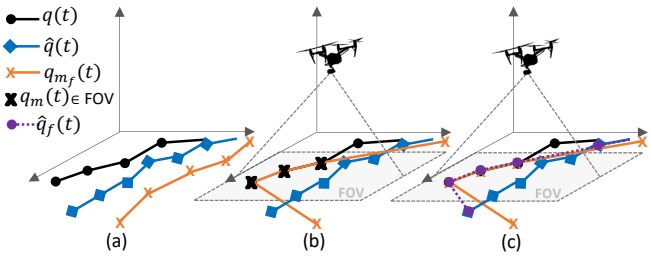

Fig. 7. Data fusion module process for a perimeter segment.

speed, and wind direction using available historical data matrices for the fire spread rate R_d, wind speed U_d, and wind direction θ_d with their respective real-time measurements, i.e., $R_m(t)$, $U_m(t)$, $\theta_m(t)$, acquired by the UAV. Before the UAV deployment, the fused input matrices are initialized with values of available historical data, i.e., $R_f = R_d$, $U_f = U_d$, $\theta_f = \theta_d$. Based on the UAV position $p(t)$ after its deployment, the fused input matrices are updated continuously with real-time measurements. In other words, the real-time measurements for fire spread rate $R_m(t)$, wind speed $U_m(t)$ WWS, and wind direction $\theta_m(t)$ are mapped based on the UAV position and their values are added accordingly to their respective fused matrices R_f, U_f, θ_f. Through this process, the spatial-temporal updated input vector $u_f = [R_f, U_f, \theta_f]$ is available to the WM module.

Data fusion is imperative to the system since it enables continuously available measurements for the perimeter state and necessary inputs to be used for the wildfire perimeter simulation, improving its accuracy significantly, as can be seen in Section **??** in the sequel.

V. SIMULATION RESULTS

We evaluated the proposed system by conducting simulation experiments in the Matlab environment. Table I includes all the parameter values used for deriving the simulation results. The rate of spread mean values μ_R are location-based, as shown on the grid of Table I, while the wind direction mean value μ_θ changes over time through the simulation. In all the simulations, the wildfire starts around [5km, 7km] while the UAV is deployed 5 minutes after the start of the fire from a depot at [1km, 1km]. Lastly, as shown in Table I, three scenarios are considered for the available historical data. Scenario A, where the historical data values (i.e., R_d, U_d, θ_d) are underestimated by 40% from the actual values (i.e., R, U, θ). Scenario B, where the historical data values are close-estimated by 5% from the actual values, and Scenario C, where the historical data values are over-estimated by 40% from the actual values.

Fig. 8 shows simulation results that illustrate the effectiveness of the proposed system for tracking the wildfire perimeter propagation in real-time. In these results, the close-estimated values (Scenario B) were used as historical data. As can be seen in Figs.8(a)-(b) and their mean error

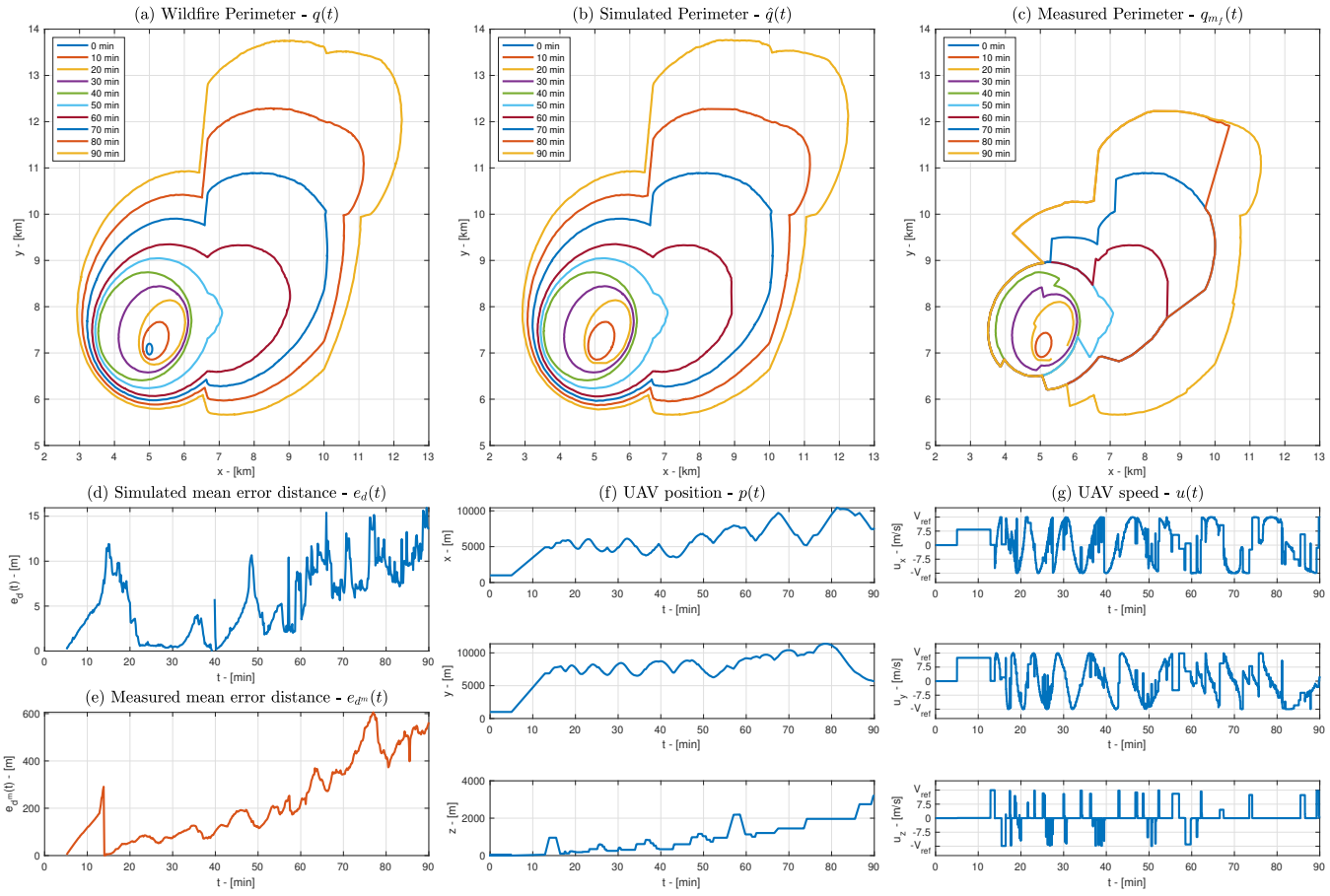

Fig. 8. Simulation results for tracking the wildfire perimeter propagation in real-time by the proposed system: Fig. 8(a) shows the actual wildfire perimeter propagation, Fig. 8(b) shows the simulated wildfire perimeter propagation by the proposed system, Fig. 8(c) shows the fused measured wildfire perimeter, Fig. 8(d) shows the mean error distance $e_d(t)$ between the wildfire perimeter in Fig. 8(a) and the simulated perimeter in Fig. 8(b), Fig. 8(e) shows the mean error distance $e_d^m(t)$ between the wildfire perimeter in Fig. 8(a) and the fused measured perimeter in Fig. 8(c), Fig. 8(f) shows the UAV position in each dimension over time, and Fig. 8(g) shows the UAV speed in each dimension over time.

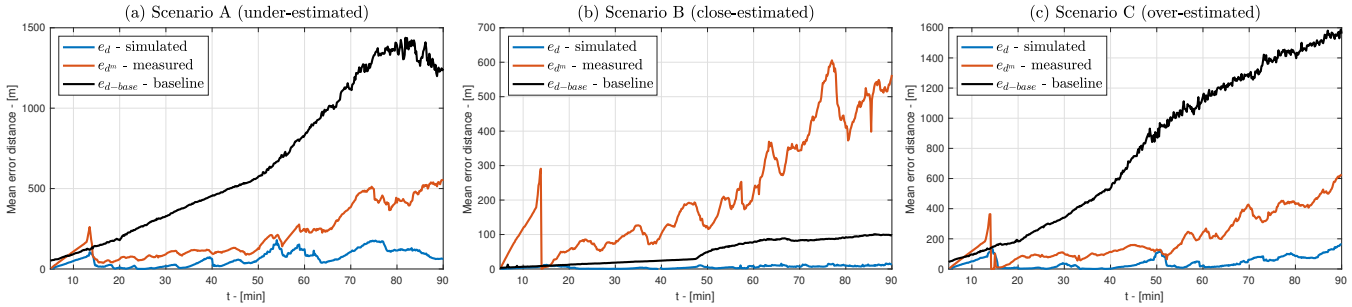

Fig. 9. The proposed system performance with different available historical data. Fig. 9(a) the proposed system uses Scenario A under-estimated data, Fig. 9(b) the proposed system uses Scenario B close-estimated data, and Fig. 9(c) the proposed system uses Scenario C over-estimated data. The baseline in each scenario is the mean error distance $e_{d\text{-base}}$ between the wildfire and a simulated perimeter obtained using only the respective historical data.

TABLE I
SIMULATION PARAMETERS VALUES

General	
Time step: $\Delta t = 1$s	Simulation time: $T = 90$min
Wildfire Model Parameters	
Grid size $[G \times G]$: $G = 20$km	Rediscr. threshold: $T_l = 35$m
Rate of spread (m min^{-1}): $R \sim \mathcal{N}(\mu_R, \sigma_R = 0.1\mu_R)$ μ_R as shown in the grid below:	Initial fire-fronts: $N_0 = 80$ Initial position: [5km, 7km] Wind speed (m s^{-1}): $U \sim \mathcal{N}(\mu_U = 2, \sigma_U = 0.2)$ Wind direction (rad): $\theta(t) \sim \mathcal{N}(\mu_\theta(t), \sigma_\theta(t)=\frac{\pi}{36})$ $\mu_\theta(0 \le t < 20) = \frac{\pi}{4}$ $\mu_\theta(20 \le t < 40) = \frac{19}{12}\pi$ $\mu_\theta(40 \le t < 60) = \frac{5}{12}\pi$ $\mu_\theta(t \ge 60) = \frac{5}{36}\pi$
UAV Parameters	
Initial position [m]: $p_0 = [1000, 1000, 0]$	Deploy time $t = 5$min Reference speed: $V_{\text{ref}} = 15$m/s
Sensor size: $S = 24$mm	Lens focal length: $F = 24$mm
Scaling factor: $s = 2$	
Historical Data	
Scenario A (under-estimated -40%): R_d=0.6R, U_d=0.6U, θ_d=0.6θ	
Scenario B (close-estimated 5%): R_d=1.05R, U_d=1.05U, θ_d=1.05θ	
Scenario C (over-estimated 40%): R_d=1.4R, U_d=1.4U, θ_d=1.4θ	

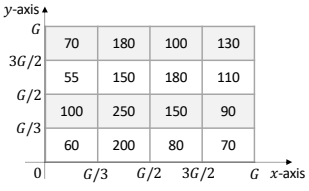

distance in Fig.8(d), the proposed system was capable of providing the state of the wildfire perimeter accurately at all times with $e_d < 17$m. Figs.8(c) shows how the single UAV was acquiring wildfire perimeter measurements and moving at different sections of the perimeter to keep the simulated perimeter as close to the actual wildfire. Lastly, Fig.8(f) shows the UAV position in the 3D space over time and Fig.8(g) its speed that is always between the provided reference speed (i.e., $V_{\text{ref}} = 15$m/s).

Fig. 9 shows simulation results comparing how the proposed system performs with different available historical data. As a baseline in each scenario, the mean error distance $e_{d\text{-base}}(t)$ is calculated between the wildfire perimeter and a simulated perimeter that is obtained using only the respective available historical data, in other words, no real-time measurements are used. As can be seen in Figs. 8(a)-(c) in all scenarios, the simulated perimeter mean error distance is significantly lower than the baseline mean error distance. We can observe that the baseline error $e_{d\text{-base}}(t)$ increases with more inaccurate historical data (i.e., Fig.9(a) and Fig.9(c)) while the proposed system although it is affected in some degree by this inaccuracy it still provides a lot more accurate results. Finally, we can observe that the measured error $e_{d^m}(t)$ is similar in all the scenarios since it is not affected directly by the historical data.

Fig. 10 shows simulation results comparing how the proposed system performs in the case of different measurement capabilities for all three scenarios. Specifically, we examine the following cases: M1 where the UAV measures only the fire-front locations q_m, M2 where also measured the spread rate R_m, M3 where measures the fire-front locations q_m and the wind speed U_m and direction θ_m, and M4 where measures everything. As can be observed, $e_d(t)$ for the M4 case is generally lower than the other cases. Moreover, the case M2 where the rate of spread is measured, provides better $e_d(t)$ than the M3 case, where the wind and direction are measured. Lastly, more inaccurate historical data provides worse $e_d(t)$ for the M1 case compared with the M4 case.

VI. CONCLUSIONS

In this paper, we propose a UAV-based system that combines the sensing capabilities of the UAV along with a wildfire propagation model to provide the real-time state of the wildfire perimeter. As described, the proposed system consists of a UAV capable of measuring the fire perimeter and also the fuel type, and the weather conditions. A wildfire model is used for providing real-time simulations of the perimeter state. The simulation perimeter values, together with the UAV perimeter measurements, are used by the wildfire perimeter tracking scheme for calculating trajectories that minimize the error between the wildfire perimeter and the simulated perimeter. A guidance and control scheme guides the UAV to follow the calculated trajectories and receive measurements. Lastly, a data fusion scheme fuses available historical data with real-time measurements providing updated inputs to the wildfire model improving its performance. The proposed system is evaluated in a

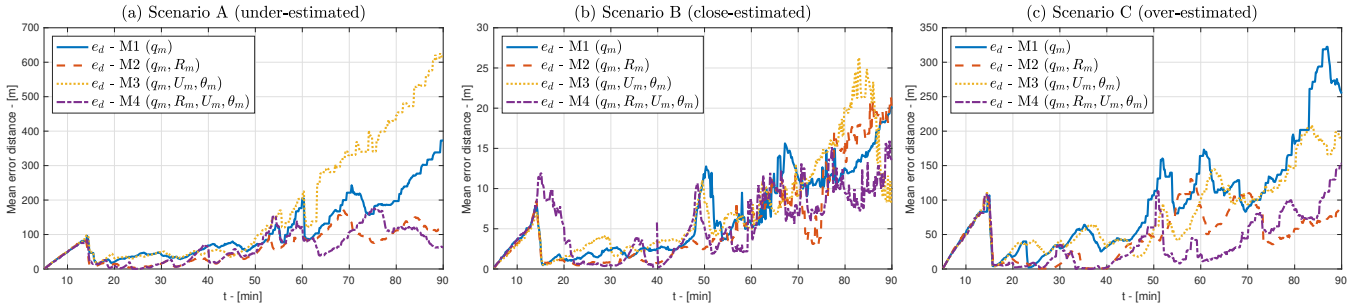

Fig. 10. The proposed system performance with different UAV measurement capabilities. Fig. 10(a) the proposed system uses Scenario A under-estimated data, Fig. 10(b) the proposed system uses Scenario B close-estimated data, and Fig. 10(c) the proposed system uses Scenario C over-estimated data.

simulation environment showcasing its ability to track the wildfire perimeter.

In the future, we plan to study the use of a small team of UAVs with the proposed system for the case of very large wildfires and also investigate the potential of extending the system for wildfire forecasting.

REFERENCES

[1] A. J. P. Smith, M. W. Jones, J. T. Abatzoglou, J. G. Canadell, and R. A. Betts, "Climate Change Increases the Risk of Wildfires," *ScienceBrief*, 2020.

[2] J. San-Miguel-Ayanz, T. Durrant, R. Boca, P. Maianti, G. Liberta, T. Artes-Vivancos, D. Oom, A. Branco, D. de Rigo, D. Ferrari, H. Pfeiffer, R. Grecchi, D. Nuijten, M. Onida, and P. Loffler, "Forest Fires in Europe, Middle East and Noth Africa 2021," *Publications Office of the European Union, Luxembourg, JRC130846*, 2022.

[3] D. W. Casbeer, D. B. Kingston, R. W. Beard, and T. W. McLain, "Cooperative forest fire surveillance using a team of small unmanned air vehicles," *International Journal of Systems Science*, vol. 37, no. 6, pp. 351–360, 2006.

[4] H. X. Pham, H. M. La, D. Feil-Seifer, and M. C. Deans, "A Distributed Control Framework of Multiple Unmanned Aerial Vehicles for Dynamic Wildfire Tracking," *IEEE Transactions on Systems, Man, and Cybernetics: Systems*, vol. 50, no. 4, pp. 1537–1548, 2020.

[5] C. Yuan, Y. Zhang, and Z. Liu, "A survey on technologies for automatic forest fire monitoring, detection, and fighting using unmanned aerial vehicles and remote sensing techniques," *Canadian Journal of Forest Research*, vol. 45, no. 7, pp. 783–792, 2015.

[6] C. Torresan, A. Berton, F. Carotenuto, S. F. Di Gennaro, B. Gioli, A. Matese, F. Miglietta, C. Vagnoli, A. Zaldei, and L. Wallace, "Forestry applications of UAVs in Europe: a review," *International Journal of Remote Sensing*, vol. 38, no. 8-10, pp. 2427–2447, 2017.

[7] F. A. Hossain, Y. Zhang, and C. Yuan, "A Survey on Forest Fire Monitoring Using Unmanned Aerial Vehicles," in *2019 3rd International Symposium on Autonomous Systems (ISAS)*, 2019, pp. 484–489.

[8] M. A. Akhloufi, A. Couturier, and N. A. Castro, "Unmanned Aerial Vehicles for Wildland Fires: Sensing, Perception, Cooperation and Assistance," *Drones*, vol. 5, no. 1, p. 15, 2021.

[9] M. Kumar, K. Cohen, and B. HomChaudhuri, "Cooperative Control of Multiple Uninhabited Aerial Vehicles for Monitoring and Fighting Wildfires," *Journal of Aerospace Computing, Information, and Communication*, vol. 8, no. 1, pp. 1–16, 2011.

[10] X. Hu, J. Bent, and J. Sun, "Wildfire Monitoring with Uneven Importance Using Multiple Unmanned Aircraft Systems," in *2019 International Conference on Unmanned Aircraft Systems (ICUAS)*, 2019, pp. 1270–1279.

[11] A. V. Savkin and H. Huang, "Navigation of a Network of Aerial Drones for Monitoring a Frontier of a Moving Environmental Disaster Area," *IEEE Systems Journal*, vol. 14, no. 4, pp. 4746–4749, 2020.

[12] E. Seraj and M. Gombolay, "Coordinated Control of UAVs for Human-Centered Active Sensing of Wildfires," in *2020 American Control Conference (ACC)*, 2020, pp. 1645–1652.

[13] C. Heracleous, P. Kolios, and C. G. Panayiotou, "An integrated UAV system for wildfire evolution monitoring and data acquisition," in *2022 International Conference on Unmanned Aircraft Systems (ICUAS)*, 2022, pp. 1131–1138.

[14] G. D. Richards, "An elliptical growth model of forest fire fronts and its numerical solution," *International Journal for Numerical Methods in Engineering*, vol. 30, pp. 1163–1179, 10 1990.

[15] G. Richards and R. Bryce, "A Computer Algorithm for Simulating the Spread of Wildland Fire Perimeters for Heterogeneous Fuel and Meteorological Conditions," *International Journal of Wildland Fire*, vol. 5, p. 73, 1995.

[16] P. L. Andrews, "The Rothermel surface fire spread model and associated developments: A comprehensive explanation," RMRS-GTR-371. Fort Collins, CO: U.S. Department of Agriculture, Forest Service, Rocky Mountain Research Station, Tech. Rep., 2018.

[17] M. A. Finney, "FARSITE: Fire Area Simulator–model development and evaluation," *Research Paper RMRS-RP-4 Revised*, 2004, Ogden, UT: U.S. Dept. Agric., Forest Service, Rocky Mountain Res. Station.

[18] J. H. Scott and R. E. Burgan, "Standard fire behavior fuel models: a comprehensive set for use with Rothermel's surface fire spread model," RMRS-GTR-153. Fort Collins, CO: U.S. Department of Agriculture, Forest Service, Rocky Mountain Research Station., Tech. Rep., 2005.